ARTICLE

Check for updates

Revealing the intrinsic superconducting gap anisotropy in surface-neutralized $BaFe_2(As_{0.7}P_{0.3})_2$

Ziming Xin[1], Yudi Wang[1], Cong Cai[1], Zhengguo Wang [1], Lei Chen[1], Tingting Han [1] & Yan Zhang [1,2 ✉]

Alkaline-earth iron arsenide (122) is one of the most studied families of iron-based super-conductors, especially for angle-resolved photoemission spectroscopy. While extensive photoemission results have been obtained, the surface complexity of 122 caused by its charge-non-neutral surface is rarely considered. Here, we show that the surface of 122 can be neutralized by potassium deposition. In potassium-coated $BaFe_2(As_{0.7}P_{0.3})_2$, the surface-induced spectral broadening is strongly suppressed, and hence the coherent spectra that reflect the intrinsic bulk electronic state recover. This enables the measuring of super-conducting gap with unpreceded precision. The result shows the existence of two pairing channels. While the gap anisotropy on the outer hole/electron pockets can be well fitted using an $s_\pm$ gap function, the gap anisotropy on the inner hole/electron shows a clear deviation. Our results provide quantitative constraints for refining theoretical models and also demonstrate an experimental method for revealing the intrinsic electronic properties of 122 in future studies.

[1] International Centre for Quantum Materials, School of Physics, Peking University, Beijing, China. [2] Collaborative Innovation Centre of Quantum Matter, Beijing, China. ✉email: yzhang85@pku.edu.cn

After the discovery of superconductivity in $LaO_{1-x}F_xFeAs$ (1111), many families of iron-based superconductor have been found, including iron-selenide (11), alkaline iron arsenide (111), alkaline-earth iron arsenide (122), etc[1,2]. Among them, the 122 family is the most studied family of iron-based superconductors, due to its high sample quality, high superconducting transition temperature (T_c), tunable carrier density, and diversity of compounds with different chemical substitutions. However, aside from these advantages, the lattice structure of 122 contains a single alkaline-earth-metal plane and hence has no charge-neutral cleavage surface (Fig. 1a, b). In $BaFe_2(As_{1-x}P_x)_2$, for example, half Ba ions are removed at the cleaved surface, and the residual Ba ions distribute inhomogeneously, forming various surface terminations[3–7]. While the alkaline-earth-metal-terminated and arsenic-terminated surfaces have been observed by scanning tunneling microscopy (STM)[4–7], the alkaline-earth-metal-deficient surface also exists with a reconstruction of alkaline-earth-metal atoms with 1×2 and $\sqrt{2} \times \sqrt{2}$ periods[6,7]. In bulk materials, one alkaline-earth-metal plane donates two electrons to the two nearest Fe–As/P planes. However, at the surface, the number of charge that transfers to the topmost Fe–As/P plane varies strongly depending on the concentration of alkaline-earth-metal atoms, leading to a charge-inhomogeneous surface for the 122 iron-based superconductors.

Angle-resolved photoemission spectroscopy (ARPES) is a powerful technique that measures the electronic structure of material in momentum space. In the studies of iron-based superconductors, ARPES plays an important role in determining band structure, Fermi surface topology, superconducting gap anisotropy, etc[8,9]. However, as a surface-sensitive technique, ARPES is very sensitive to the cleavage surface of material. For example, in 1111, the separation of bulk and surface states has been observed, which was attributed to the charge-non-neutral cleavage surface of 1111 (refs. [10–12]). However, for the most studied family of iron-based superconductors, the 122 family, the complexity caused by its charge-non-neutral surface is rarely considered. While few theories and experiments show the possible existence of surface state in 122 (refs. [3,13]), the photoemission spectra taken in 122 are generally much broader[13–20] than that taken in other families of iron-based superconductors[21–25]. Such broadening behavior and its origin have not been well understood so far.

Here, we report the measurement of gap anisotropy in an optimal-doped 122 compound $BaFe_2(As_{0.7}P_{0.3})_2$ utilizing ARPES and in situ potassium deposition. We find that by depositing a small amount of potassium on the sample surface, the spectra become sharp and coherent, which allows us to measure the superconducting gap anisotropy on all Fermi surface sheets with unpreceded precision. We show that the obtained gap anisotropy cannot be fitted using a single $|\cos k_x \cos k_y|$ gap function, but could be explained by the nesting- and orbital-selectivity of the superconducting pairing. Our detailed and precise gap measurement provide crucial clues for uncovering the paring mechanism of iron-based superconductors. It also implies that the surface complexity of 122 needs to be seriously considered. The potassium deposition can be used as a practical experiment method for revealing the intrinsic electron structure and gap anisotropy of 122 iron-based superconductors in the future studies.

Results

Evolution of electronic structure in potassium-coated $BaFe_2(As_{0.7}P_{0.3})_2$. The Fermi surface mappings taken in the pristine and doped samples are compared in Fig. 1c, d. The photoemission spectra distribute broadly in the pristine sample (D0) and shadow Fermi pockets are observed at the Brillouin zone boundary (X), indicating a 1×2 reconstruction of the cleavage surface. With potassium deposition, the sharpening of photoemission spectra is obvious. Two hole pockets (α and β) and two electron pockets (δ and η) are now clearly resolved at the Brillouin zone center (Γ) and zone corner (M). The sharpness of photoemission spectra taken in the doped sample transcends
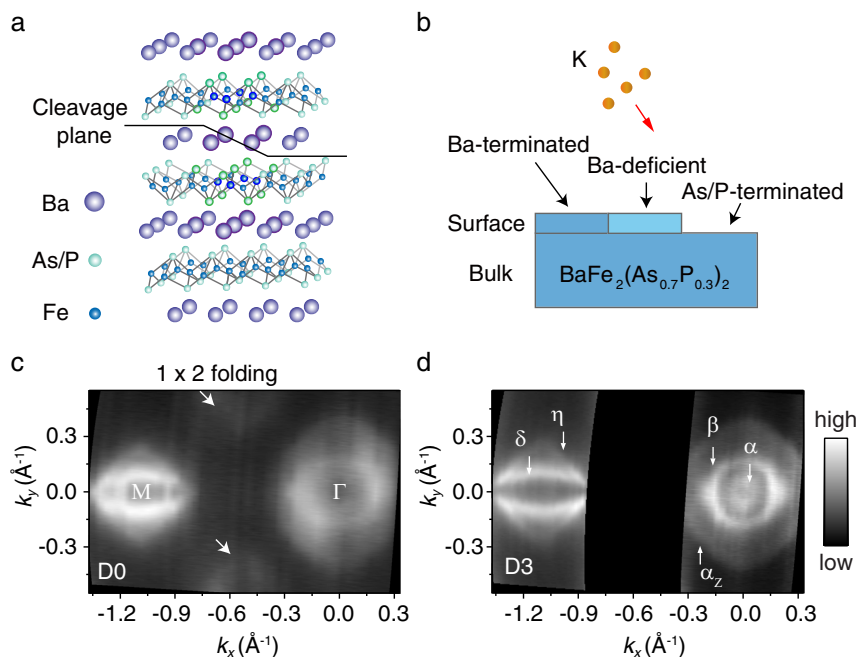

Fig. 1 Surface complexity of $BaFe_2(As_{0.7}P_{0.3})_2$. a Schematic drawing of the lattice structure of $BaFe_2(As_{0.7}P_{0.3})_2$. The black solid line illustrates the position of a possible cleavage plane. **b** Schematic drawing of the cleavage surface and potassium deposition. **c** Fermi surface mapping taken in the pristine sample (D0). k_x and k_y are the momenta of electrons along x and y directions. Panel **d** is the same as **c** but taken in the doped sample (D3) after three times potassium deposition.
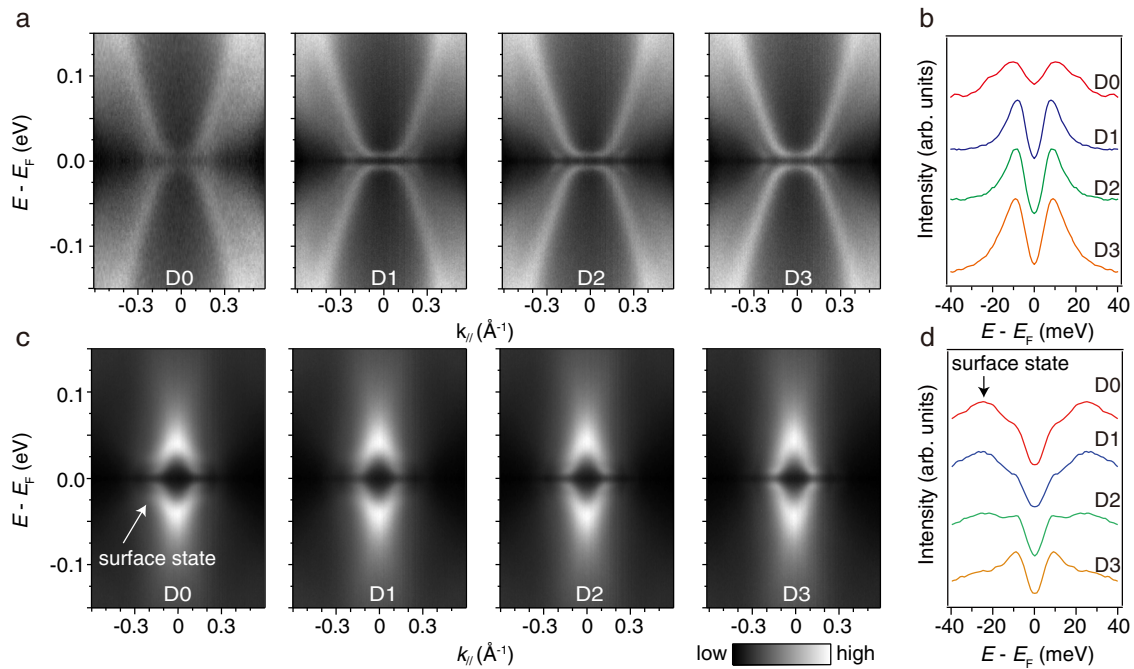
Fig. 2 Band evolution in potassium-coated BaFe$_2$(As$_{0.7}$P$_{0.3}$)$_2$. a Doping dependence of the symmetrized energy-momentum cuts taken around the Γ point. $E-E_F$ represents the binding energy of electrons. E is the kinetic energy of electrons and E_F is the Fermi energy. $k_{//}$ is the in-plane momentum of electrons. **b** Doping dependence of the symmetrized energy distribution curves (EDCs) taken at the Fermi crossing (k_F) of the α hole band. Panels **c** and **d** are the same as **a** and **b** but taken around the M point. The EDCs are taken at the k_F of the δ electron band. The deposition sequence is denoted using Dn (n is the doping times).

most previous ARPES studies on 122, especially for the Fermi surface mapping taken around the M point[8,9,14–17]. Note that, the large hole pocket (α_Z) is a shadow Fermi pocket that is folded from the Z point due to the finite k_z resolution of ARPES[17].

To further show the effect of potassium deposition, we take the energy-momentum cuts across the hole/electron pockets and plot their doping dependence in Fig. 2. Around the Γ point, the spectra become sharper with potassium deposition (Fig. 2a), and meanwhile the superconducting peaks become more coherent (Fig. 2b). Around the M point, a surface band could be observed at around -20 meV as pointed out by the white arrow (Fig. 2c). With potassium deposition, this surface band weakens and eventually diminishes. As a result, the superconducting coherent peak is clearly resolved (Fig. 2d). It should be noted that, we could not resolve any change of Fermi crossings (k_Fs) and gap magnitudes (Δ), which indicates that the total potassium coverage is very low. Based on our energy and momentum resolutions, we could set an upper bound of total potassium coverage to be ~0.015 ML. For each doping step, the increment of potassium coverage is estimated to be below 0.005 ML. Such small amount of potassium is sufficient to improve the spectral quality while having little influence on band structure and superconductivity.

Superconducting gap anisotropy in potassium-coated BaFe$_2$(As$_{0.7}$P$_{0.3}$)$_2$. Being able to resolve the intrinsic ARPES spectra is critical for the quantitative spectra analysis. The sharpness of spectra taken in potassium-coated BaFe$_2$(As$_{0.7}$P$_{0.3}$)$_2$ is now comparable with that taken in 11 and 111 iron-based superconductors[21–25] (Supplementary Fig. 1). On one hand, the effective mass and lifetime of quasiparticles could be determined more accurately, which is important for studying the quantum critical phenomena of BaFe$_2$(As$_{1-x}$P$_x$)$_2$ (refs. [26,27]). On the other hand, the superconducting coherent peaks are well defined on all Fermi surface sheets, which allows us to measure the superconducting gap anisotropy with unpreceded precision. The results

are shown in Fig. 3. The superconducting gap is nearly isotropic on the α and β hole pockets (Δ_α and Δ_β) (Fig. 3a–d), but shows moderate anisotropy on the δ and η electron pockets (Δ_δ and Δ_η) (Fig. 3e–h). For Δ_δ, the gap reaches maximum at 90°, while for Δ_η, the gap maxima locate at 45° and 135°.

Figure 4 summarizes the angular distributions of superconducting gap on all Fermi surface sheets. It is commonly believed that the pairing symmetry of 122 is an s$_\pm$-wave[28–31] and the superconducting gap anisotropy can be fitted using a $\Delta_0|$cos$k_x$cos$k_y|$ gap function[16,18–20]. Here, our detailed and precise gap measurements allow us to test the validity of s$_\pm$ gap function quantitatively. We fitted the data using the experimental determined Fermi surface (Fig. 4a) and summarized the fitting results in Fig. 4b–f. For the superconducting gap anisotropies on the β and η pockets, the four-fold symmetry of Δ_η and the relative gap magnitudes of Δ_β and Δ_η can be well described by the s$_\pm$ gap function with $\Delta_0 = 8.7$ meV. However, for the α and δ pockets, the superconducting gap clearly deviates from the s$_\pm$ gap function with a larger gap magnitude, which indicates a stronger superconducting pairing on the α and δ pockets.

Discussion
We first discuss how the potassium atoms play roles on the surface of BaFe$_2$(As$_{1-x}$P$_x$)$_2$. There are several possible scenarios. First, electrons transfer from the potassium atoms to the sample surface, which neutralizes the charge-non-neutral surface, leading to a suppression of the surface broadening effect. Second, the potassium atoms could act as a catalyzer which causes the redistribution of alkaline-earth-metal atoms on the sample surface in a more homogeneous way. Third, the potassium atoms scatter electrons at the sample surface. The surface electronic states then turn into an incoherent and continuous background that is inconspicuous in photoemission spectra. To understand the mechanism of potassium deposition, further experimental and theoretical studies are required. Nevertheless, our results
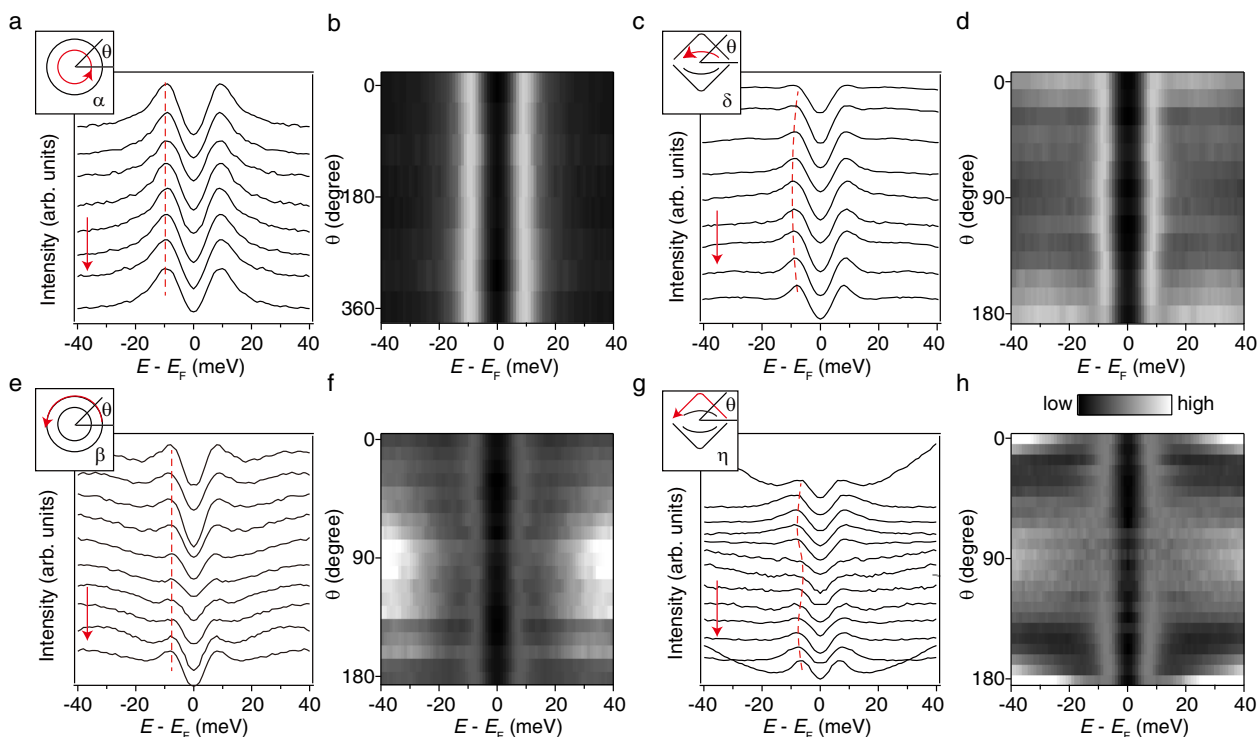
Fig. 3 Angular distributions of superconducting gap on Fermi surface sheets. a Angle dependence of the symmetrized energy distribution curves (EDCs) taken on the α hole pocket. The red dashed line guides the eyes to the gap anisotropy. $E-E_F$ represents the binding energy of electrons. E is the kinetic energy of electrons and E_F is the Fermi energy. The red arrow illustrates the direction of the data presentation. **b** The merged image of the symmetrized EDCs for better visualizing the gap anisotropy. The polar angle (θ) is defined in **a**. Panels **c**, **d**, **e**, **f**, **g**, and **h** are the same as **a** and **b**, but taken on the δ, β, and η pockets, respectively. All data were taken in the D3 sample at 8 K.
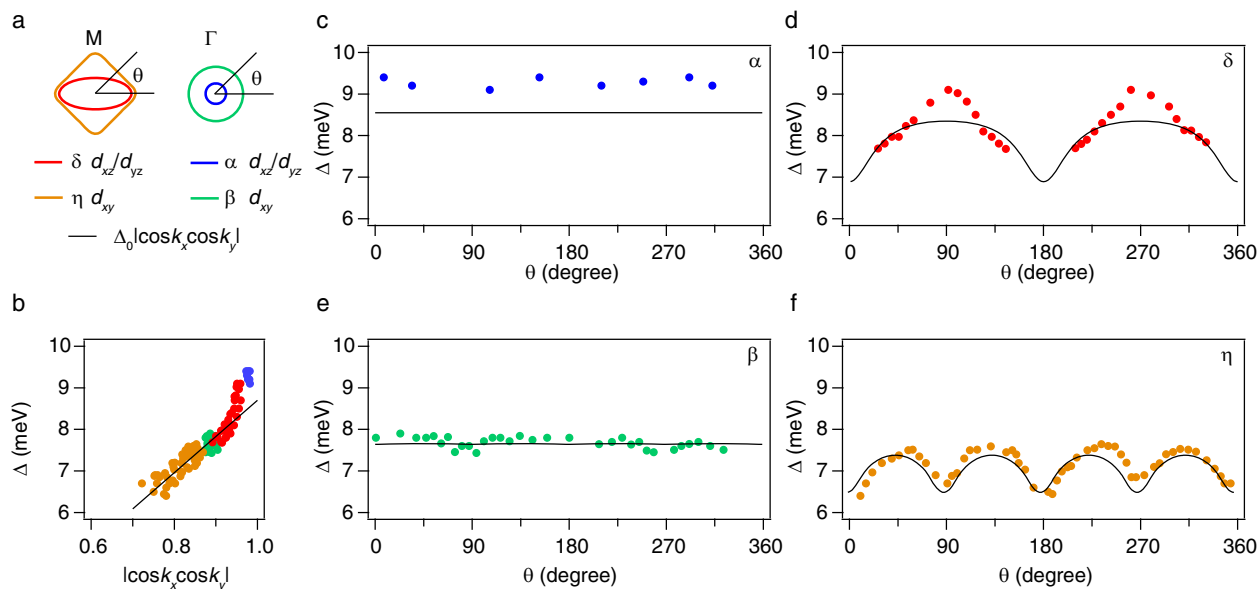

Fig. 4 Superconducting gap fitting using an $s_\pm$ gap function. a Schematic drawing of the Fermi surface of $BaFe_2(As_{0.7}P_{0.3})_2$. The orbital characters of Fermi surface are illustrated using different colors[14,17,18,39,40]. **b** Plot of the superconducting gap (Δ) as a function of $|\cos k_x \cos k_y|$. **c** Angular distribution of the superconducting gap on the α pocket. The polar angle (θ) is defined in **a**. Panels **d**, **e**, and **f** are the same as **c** but taken on the δ, β, and η pockets, respectively. The black solid lines in all panels are the best fit using the gap function $\Delta_0|\cos k_x \cos k_y|$ with $\Delta_0 = 8.7$ meV.

highlight the surface complexity of 122 iron-based super-conductors. This implies that previous photoemission results taken on 122 should be carefully revisited.

For example, ARPES observed double peak features in $Ba_{1-x}K_xFe_2As_2$, whose origin remains controversial[32–35]. Some

attribute it to the band degeneracy[32,33], while others believe it is originated from the electron-bosonic coupling[34] or in-gap impurity state[35]. Moreover, ARPES data taken on $BaFe_2As_2$, $SrFe_2As_2$, $CaFe_2As_2$, etc.[36–38] show complex band structures. The number of bands observed by ARPES is inconsistent with the

band calculations. Here, we show that the surface complexity might explain these controversial behaviors of 122 iron-based superconductors. The possible existence of surface-related features could be easily verified using potassium deposition. For $BaFe_2(As_{1-x}P_x)_2$, its nodal location is still under debate[18,39–41]. We measured the k_z dependence of superconducting gap in the D3 sample (Supplementary Fig. 2). While our high-quality data confirm the existence of gap nodes on the hole pockets around the Z point[18], no gap node is resolved on the electron pockets. Although we cannot fully exclude the possible existence of nodal loop on electron pockets due to our finite k_z resolution, we show that the data quality can be significantly improved by potassium deposition especially for the gap measurement on the electron pockets. With a more bulk-sensitive and comprehensive photon energy dependent experiment, it can be determined whether the nodal loop exists or not.

We now turn to the in-plane superconducting gap anisotropy, which has been studied by ARPES for many iron-based superconductors. For 111 and 11 compounds, such as LiFeAs, $NaFe_{1-x}Co_xAs$ and FeSe, the Fermi pockets are small and the T_cs are relatively low, making the gap function fitting unreliable and unable to provide effective information[8,23–25]. For 122 compounds, due to the surface broadening effect, the superconducting gap anisotropy, especially the gap anisotropy on the electron pockets, has never been resolved clearly. Here, we achieve an accurate and reliable gap measurement of 122 using potassium-coated $BaFe_2(As_{0.7}P_{0.3})_2$. Taking all advantages of 122, such as large Fermi pocket size and high T_c, our data provide an ideal touchstone for testing the theoretical models of iron-based superconductors.

First, we show that the superconducting pairing cannot be described by a single $s_\pm$ pairing channel, but instead consists of at least two pairing channels. One pairing channel follows the $s_\pm$ pairing symmetry and dominates the superconducting pairing on the β and η pockets. The other pairing channel could be described as a second $s_\pm$ pairing channel with a larger gap pre-factor. It dominates the superconducting pairing on the α and δ pockets. Our results undoubtedly show that the single gap function that normally describes a single band superconductor fails to explain the gap anisotropy of iron-based superconductors. The existence of multiple pairing channels and the interplays among them should be considered in the description of pairing interactions in iron-based superconductors.

Second, according to the theories of iron-based superconductors[28–31], the pair scattering of electrons is mediated by a large **Q** scattering that connects the Fermi pockets at the Γ and M points. Here, our gap fitting shows that two pair scattering channels connect the outer electron and hole pockets (β and η) and the inner electron and hole pockets (α and δ), respectively. On one hand, the outer hole and electron pockets are similar in size and are well nested. This is also the case for the inner hole and electron pockets. The nesting of Fermi surface naturally separates out two pair scattering channels which locate respectively on the outer and inner Fermi pockets. On the other hand, while the β and η pockets are constructed by the d_{xy} orbital, the α and δ pockets are constructed by the d_{xz}/d_{yz} orbitals. The intra-orbital pair scattering could also lead to a separation of two pairing channels respectively from the d_{xz}/d_{yz} and d_{xy} orbitals. Based on above discussions, our results indicate that the intra-orbital pair scattering between two nested Fermi pockets plays a dominating role in the superconducting pairing of iron-based superconductors. As a result, the superconducting pairing becomes nesting- and orbital-selective[42,43]. By fitting the gap anisotropy using a more complex and parameterized gap function, the detailed momentum and orbital dependence of pairing

interactions could be obtained, which would help to construct an accurate and realistic superconducting pairing model for iron-based superconductors.

In summary, we report the superconducting gap measurement in potassium-coated $BaFe_2(As_{0.7}P_{0.3})_2$. We found that a small amount of potassium deposition could suppress the surface-broadening effect and help us to reveal the intrinsic electron structure of $BaFe_2(As_{0.7}P_{0.3})_2$. Our high quality and precise gap measurement distinguishes two pairing channels, which unveils the nesting- and orbital-selective nature of the superconducting pairing of iron-based superconductors. Our results show that the surface-neutralization enables the photoemission data taken in 122 to be analyzed with unpreceded precision. The results would provide crucial clues for uncovering the pairing mechanism of iron-based superconductors.

Methods

Sample preparations. High-quality $BaFe_2(As_{0.7}P_{0.3})_2$ single crystals were grown using self-flux method[44]. Ba_2As_3, Ba_2P_3, FeAs, FeP were starting materials, which were mixed at a molar ratio of 2.82 : 0.18 : 0.94 : 0.06, placed in an Al_2O_3 crucible, and sealed in an iron crucible. The crucible was heated at 1150 °C for 10 h, and then the temperature cooled down to 900 °C at a rate of 1 °C per hour. Finally, 1 mm × 1 mm × 0.2 mm high-quality single crystal can be obtained. The T_c is around 30 K as confirmed by magnetic susceptibility measurement.

Angle-resolved photoemission spectroscopy. The ARPES data were taken at Stanford synchrotron radiation lightsource (SSRL) beamline 5–4. The photon energy is 23 eV. The overall energy resolution is around 5 meV and the angular resolution is around 0.3°. The samples were cleaved in situ and measured in vacuum better than 5×10^{-10} mbar. All data were measured at 8 K. The potassium deposition was conducted in situ using a potassium dispenser. We repeated the deposition several times. The deposition sequence is denoted using Dn (n is the doping times). The current of the potassium dispenser is ~5.4 A, and each deposition last for ~8 s.

Data availability
Data that support the findings of this study are available upon reasonable request from the corresponding authors.

References
1. Stewart, G. R. Superconductivity in iron compounds. *Rev. Mod. Phys.* **83**, 1589–1652 (2011).
2. Paglione, J. & Greene, R. L. High-temperature superconductivity in iron-based materials. *Nat. Phys.* **6**, 645–658 (2010).
3. Gao, M., Ma, F., Lu, Z.-Y. & Xiang, T. Surface structures of ternary iron arsenides AFe_2As_2 (A=Ba, Sr, or Ca). *Phys. Rev. B* **81**, 193409 (2010).
4. Nascimento, V. B. et al. Surface geometric and electronic structure of $BaFe_2As_2$(001). *Phys. Rev. Lett.* **103**, 076104 (2009).
5. Yin, J.-X. et al. Orbital selectivity of layer-resolved tunneling in the iron-based superconductor $Ba_{0.6}K_{0.4}Fe_2As_2$. *Phys. Rev. B* **102**, 054515 (2020).
6. Niestemski, F. C. et al. Unveiling the atomic and electronic structure at the surface of the parent pnictide $SrFe_2As_2$. Preprint at https://arxiv.org/abs/0906.2761 (2009).
7. Li, A. et al. Surface terminations and layer-resolved spectroscopy in 122 iron pnictide superconductors. *Phys. Rev. B* **99**, 134520 (2019).
8. Richard, P., Sato, T., Nakayama, K., Takahashi, T. & Ding, H. Fe-based superconductors: an angle-resolved photoemission spectroscopy perspective. *Rep. Prog. Phys.* **74**, 124512 (2011).
9. Ye, Z.-R., Zhang, Y., Xie, B.-P. & Feng, D.-L. Angle-resolved photoemission spectroscopy study on iron-based superconductors. *Chin. Phys. B* **22**, 087407 (2013).
10. Liu, C. et al. Surface-driven electronic structure in LaFeAsO studied by angle resolved photoemission spectroscopy. *Phys. Rev. B* **82**, 075135 (2010).
11. Zhang, P. et al. Disentangling the surface and bulk electronic structures of LaOFeAs. *Phys. Rev. B* **94**, 104517 (2016).
12. Yang, L. X. et al. Surface and bulk electronic structures of LaFeAsO studied by angle-resolved photoemission spectroscopy. *Phys. Rev. B* **82**, 104519 (2010).

13. Pfau, H. et al. Detailed band structure of twinned and detwinned BaFe$_2$As$_2$ studied with angle-resolved photoemission spectroscopy. *Phys. Rev. B* **99**, 035118 (2019).
14. Zhang, Y. et al. Orbital characters of bands in the iron-based superconductor BaFe$_{1.85}$Co$_{0.15}$As$_2$. *Phys. Rev. B* **83**, 054510 (2011).
15. Yi, M. et al. Symmetry-breaking orbital anisotropy observed for detwinned Ba (Fe$_{1-x}$C$_{ox}$)As$_2$ above the spin density wave transition. *Proc. Natl Acad. Sci. USA* **108**, 6878–6883 (2011).
16. Terashima, K. et al. Fermi surface nesting induced strong pairing in iron-based superconductors. *Proc. Natl Acad. Sci. USA* **106**, 7330–7333 (2009).
17. Ye, Z.-R. et al. Doping dependence of the electronic structure in phosphorus-doped ferropnictide superconductor BaFe$_2$(As$_{1-x}$P$_x$)$_2$ studied by angle-resolved photoemission spectroscopy. *Phys. Rev. B* **86**, 035136 (2012).
18. Zhang, Y. et al. Nodal superconducting-gap structure in ferropnictide superconductor BaFe$_2$(As$_{0.7}$P$_{0.3}$)$_2$. *Nat. Phys.* **8**, 371–375 (2012).
19. Ding, H. et al. Observation of Fermi-surface-dependent nodeless superconducting gaps in Ba$_{0.6}$K$_{0.4}$Fe$_2$As$_2$. *Europhys. Lett.* **83**, 470031 (2008).
20. Nakayama, K. et al. Superconducting gap symmetry of Ba$_{0.6}$K$_{0.4}$Fe$_2$As$_2$ studied by angle-resolved photoemission spectroscopy. *Europhys. Lett.* **85**, 67002 (2009).
21. Watson, M. D. et al. Evidence for unidirectional nematic bond ordering in FeSe. *Phys. Rev. B* **94**, 201107 (2016).
22. Zhang, Y. et al. Distinctive momentum dependence of the band reconstruction in the nematic state of FeSe thin film. *Phys. Rev. B* **94**, 115153 (2016).
23. Miao, H. et al. Isotropic superconducting gaps with enhanced pairing on electron Fermi surfaces in FeTe$_{0.55}$Se$_{0.45}$. *Phys. Rev. B* **85**, 094506 (2012).
24. Borisenko, S. V. et al. Superconductivity without nesting in LiFeAs. *Phys. Rev. Lett.* **105**, 067002 (2010).
25. Umezawa, K. et al. Unconventional anisotropic s-wave superconducting gaps of the LiFeAs iron-pnictide superconductor. *Phys. Rev. Lett.* **108**, 037002 (2012).
26. Kasahara, S. et al. Evolution from non-Fermi- to Fermi-liquid transport via isovalent doping in BaFe$_2$(As$_{1-x}$P$_x$)$_2$ superconductors. *Phys. Rev. B* **81**, 184519 (2010).
27. Walmsley, P. et al. Quasiparticle mass enhancement close to the quantum critical point in BaFe$_2$(As$_{1-x}$P$_x$)$_2$. *Phys. Rev. Lett.* **110**, 257002 (2013).
28. Hirschfeld, P. J., Korshunov, M. M. & Mazin, I. I. Gap symmetry and structure of Fe-based superconductors. *Rep. Prog. Phys.* **74**, 124508 (2011).
29. Wang, F. & Lee, D.-H. The electron-pairing mechanism of iron-based superconductors. *Science* **332**, 200–204 (2011).
30. Dai, P., Hu, J. & Dagotto, E. Magnetism and its microscopic origin in iron-based high-temperature superconductors. *Nat. Phys.* **8**, 709–718 (2012).
31. Mazin, I. I. & Schmalian, J. Pairing symmetry and pairing state in ferropnictides: theoretical overview. *Physica C* **469**, 614–627 (2009).
32. Xu, Y.-M. et al. Observation of a ubiquitous three-dimensional superconducting gap function in optimally doped Ba$_{0.6}$K$_{0.4}$Fe$_2$As$_2$. *Nat. Phys.* **7**, 198–202 (2011).
33. Zhang, Y. et al. Out-of-plane momentum and symmetry-dependent energy gap of the pnictide Ba$_{0.6}$K$_{0.4}$Fe$_2$As$_2$ superconductor revealed by angle-resolved photoemission spectroscopy. *Phys. Rev. Lett.* **105**, 117003 (2010).
34. Shimojima, T. et al. Anomalous two peak structure in the angle-resolved photoemission spectra of Ba$_{1-x}$K$_x$Fe$_2$As$_2$. Preprint at https://arxiv.org/abs/1206.3163 (2012).
35. Zhang, P. et al. Observation of momentum-confined in-gap impurity state in Ba$_{0.6}$K$_{0.4}$Fe$_2$As$_2$: evidence for anti-phase s$_\pm$ pairing. *Phys. Rev. X* **4**, 031001 (2014).
36. Yi, M. et al. Unconventional electronic reconstruction in undoped (Ba, Sr) Fe$_2$As$_2$ across the spin density wave transition. *Phys. Rev. B* **80**, 174510 (2009).
37. Zhang, Y. et al. Unusual doping dependence of the electronic structure and coexistence of spin-density-wave and superconductor phases in single crystalline Sr$_{1-x}$K$_x$Fe$_2$As$_2$. *Phys. Rev. Lett.* **102**, 127003 (2009).
38. Wang, Q. et al. Symmetry-broken electronic structure and uniaxial Fermi surface nesting of untwinned CaFe$_2$As$_2$. *Phys. Rev. B* **88**, 235125 (2017).
39. Suzuki, K., Usui, H. & Kuroki, K. Possible three-dimensional nodes in the s$_\pm$ superconducting gap of BaFe$_2$(As$_{1-x}$P$_x$)$_2$. *J. Phys. Soc. Jpn.* **80**, 013710 (2011).
40. Yoshida, T. et al. Two-dimensional and three-dimensional fermi surfaces of superconducting BaFe$_2$(As$_{1-x}$P$_x$)$_2$ and their nesting properties revealed by angle-resolved photoemission spectroscopy. *Phys. Rev. Lett.* **106**, 117001 (2013).
41. Yoshida, T. et al. Anisotropy of the superconducting gap in the iron-based superconductor BaFe$_2$(As$_{0.7}$P$_{0.3}$)$_2$. *Sci. Rep.* **4**, 7292 (2014).
42. Sprau, P. O. et al. Discovery of orbital-selective Cooper pairing in FeSe. *Science* **357**, 75–80 (2017).
43. Kreisel, A. et al. Orbital selective pairing and gap structures of iron-based superconductors. *Phys. Rev. B* **95**, 174504 (2017).
44. Nakajima, M. et al. Growth of BaFe$_2$(As$_{1-x}$P$_x$)$_2$ single crystals (0≤x≤1) by Ba$_2$As$_3$/Ba$_2$P$_3$-flux method. *J. Phys. Soc. Jpn.* **81**, 104710 (2012).

Author contributions
Y.Z. conceived and instructed the project. Z.M.X. synthesized the single crystals. Y.D.W. took the ARPES measurements with the contribution of T.T.H., C.C., Z.G.W., L.C., and Z.M.X. Z.M.X. and Y.Z. analyzed the data and wrote the paper with the input from all authors.

Competing interests
The authors declare no competing interests.

Additional information
Supplementary information The online version contains supplementary material available at https://doi.org/10.1038/s42005-021-00537-z.

Correspondence and requests for materials should be addressed to Y.Z.

Reprints and permission information is available at http://www.nature.com/reprints

Publisher's note Springer Nature remains neutral with regard to jurisdictional claims in published maps and institutional affiliations.